Energy and Buildings 133 (2016) 131–140

Contents lists available at ScienceDirect

Energy and Buildings

journal homepage: www.elsevier.com/locate/enbuild

Experimental investigation and numerical validation of total heat exchanger and membrane phenomena

S. Sabek[a,*], F. Tiss[a], R. Chouikh[b], A. Guizani[a]

[a] Thermal Process Laboratory Research and Technologies Centre of Energy, Borj-Cedria Science and Technologies Park, BP 95, 2050 Hammam-lif, Tunisie
[b] King Khalid University, Faculty of Science, Physics Department, P. O. Box 9004, Abha 61413, Saudi Arabia

ARTICLE INFO

Article history:
Received 26 December 2015
Received in revised form 10 June 2016
Accepted 20 September 2016
Available online 21 September 2016

Keywords:
Total heat exchanger
Membrane phenomena
Efficiency

ABSTRACT

The total heat exchanger is a promising technology used to recover both latent and sensible heat. An experimental setup was built in order to evaluate parametric effects on the total heat exchanger efficiency. Numerically, the physical problem involves a two dimensional model including the momentum, heat and mass transport equations in climate chamber submitted to a fresh air stream. The impact of air flow velocity on the heat and mass transfer distributions are experimentally and numerically established. The results show that the air temperature inside the climate chamber decreases from 19.5 to 17.6 °C when the air flow velocity increases from 0.125 m s^{-1} to 0.25 m s^{-1}. The surface of membrane has a great impact on the temperature and humidity profiles inside climate chamber when the membrane surface is sufficiently large. Complex phenomena such activation and clogging of membrane are discussed. The variation of membrane surface and/or flow velocity has an important impact on the activation and clogging times.

1. Introduction

Total Heat Exchangers (THEs) have received significant progress in the past twenty years and they are estimated to play an essential role in building air conditioning installations [1,3]. Comparing to sensible heat exchangers, THEs have the benefit to ameliorate significantly the quality of breathing air coming from outside and can be more efficient than habitual filters.

THEs efficiency is directly related to both membrane design and property. Their ability to recover moisture and sensible heat in the exchanger is responsible for its overall performance. Therefore, membrane being a thin and flexible material manages the transport of vapor water and dry air from side to other of the building. The transport of vapor water depends on the membrane type and morphological properties such as thickness, thermal conductivity, mass diffusivity and porosity as discussed by [4,5].

Water management is fundamental to improve the performance and efficiency of the THEs. Therefore, it is significant to understand the effect of water condensation on the transport properties of the hydrophobic membrane, especially at low temperature.

Inside building, the water is present in vapor phase. The liquid water droplets formed by condensation must be removed because it may block the pores of the membrane resulting in a decrease of mass and heat transport outward.

Several previous researches showed that the performance of THEs is not only impacted by parameters related to the building such as outdoor temperature and indoor air conditions, but also by THEs design and membrane properties [6,7]. These researches have been carried out to investigate the flow arrangement effects such as co current, counter current, cross flow and quasi counter flow on the THEs efficiency [8,9]. During the past decade, researches were mainly focused on material characteristics used in THEs such as Nafion [10], cellulose triacetate [11], polyether-polyurethane [12], polyethersulfone [13], PolyVinylidene FluoriDe (PVFD), and polystyrene-sulfonate [14]. Zhang et al. [15] tested an asymmetric cellulose acetate membrane synthesized using the wet phase inversion method for total heat recovery. Their results show that the additive water has a strong impact on both membrane surface structure and performance. Zhang et al. [16] fabricated a new composite membrane which used polyethersulfone as a support layer and a dense polyvinyl alcohol as the active separator layer in order to facilitate and improve the water vapor permeability in air dehumidification process. They concluded that the addition of lithium chloride salts can enhance vapor permeability and membrane hydrophobicity. Ye et al. [17] studied the permeability of Nafion membrane to the water vapor using an effective mathematical model for air drying application. Their numerical and experimental results show that the membrane permeability depends essentially

* Corresponding author.
E-mail address: seifennasr.sabek@gmail.com (S. Sabek).

http://dx.doi.org/10.1016/j.enbuild.2016.09.045
0378-7788/

Nomenclature

D_v	Vapor diffusivity ($m^2\,s^{-1}$)
D_h	Hydraulic diameter (m)
f	Darcy friction factor
H	Height of total heat exchanger (m)
K	Permeability (m^2)
l_{THE}	Width of total heat exchanger (m)
L_{THE}	Length of total heat exchanger (m)
n	Normal vector
n*	Dimensionless normal vector
p	Pressure (Pa)
p*	Dimensionless pressure $p^* = \frac{p}{\rho_a {u_0}^2}$
Pr	Prandtl number$Pr = \frac{\nu}{\alpha}$
Re	Reynolds number$Re = \frac{u_0 D_h}{\nu}$
Sc	Schmidt number$Sc = \frac{\nu}{D_v}$
T	Temperature (K)
u, v	Velocity ($m\,s^{-1}$) for x and y directions respectively
u*, v*	Dimensionless velocities $\left(u^* = \frac{u}{u_0}, v^* = \frac{v}{u_0}\right)$
u_0	Inlet velocity ($m\,s^{-1}$)
x, y	Coordinates (m)
x*, y*	Dimensionless coordinates $\left(x^* = \frac{x}{H}, y^* = \frac{y}{H}\right)$

Greek letters

α	Thermal diffusivity ($m^2\,s^{-1}$)
ε	Efficiency
ξ	Dimensionless humidity
θ	Dimensionless temperature
ρ_a	Air density ($kg\,m^{-3}$)
ω	Humidity ratio ($kg\,kg^{-1}$)
ν	Kinematic viscosity ($m^2\,s^{-1}$)

Subscripts

f	Fresh air
i	Inlet
l	Latent
m	Membrane
s	Sensible

on its thickness and its sensibility to the water vapor pressure in the gas phase. Recently, Yang et al. [18] investigated experimentally a quasi-counter flow parallel plate membrane contactor for air drying application. They specified that PVDF membrane has the highest humidification efficiency. From the design view point, they concluded that its efficiency is lower than counter flow exchanger and higher than the cross flow one.

Among various membrane types, Nafion membrane has gained popularity among scientists and engineers because of its high moisture permeability, great thermal conductivity and good mechanical rigidity. This membrane is separated into hydrophobic areas covered of tetrafluoroethylene and sulfonic acid groups. However, at low temperatures, excess vapor water condensation in the porous structure of the membrane can obstruct the humid air transport by diffusion from inside to outside of the building via the fresh air channel. The liquid water condensed at the outer surface of THEs membrane created another physical phenomenon known as the membrane clogging [19,20].

In the literature, there are notable absences of the integration of this technology in buildings due to the difficulties of accompanied phenomena (activation and clogging). For this purpose, a special room, in which the dimensions change proportionally with the membrane surface area, needs to be created. This technique is applied by Korjenic et al. [21] to evaluate the moisture buffering and moisture recovery conditions in order to reduce the energy demand and the CO_2 emission of a building.

Table 1
Geometrics properties of Total Heat Exchanger.

	Values	Unit
L_{THE}	$50\ 10^{-2}$	m
l_{THE}	$45\ 10^{-2}$	m
H	$22\ 10^{-2}$	m
$V_{climate\ chamber}$	$33.00\ 10^{-3}$	m^3
$V_{fresh\ air\ channel}$	$16.50\ 10^{-3}$	m^3

Several numerical models have been developed to predict the heat and moisture transport near the membrane of THEs, which contributed extensively to appreciate water vapor transport along the porous zone [22–26]. However, these models are focused only to investigate effects of design and membrane type on the performance of THEs but rarely considered their utilization in building construction.

In this paper, the system under investigation considers a counter-current configuration of THEs using Nafion membrane. This study focuses on both heat and moisture transport in the climate chamber as well as on the observable fact such as activation and clogging phenomenon occurring in the porous membrane. For this purpose, an experimental prototype of membrane incorporated in climate chamber is constructed in order to investigate several operating situations related to the membrane and the interior special room characteristics.

The purpose of this paper is to investigate experimentally and to validate numerically the feasibility and the performance of the THEs in the considered chamber. Three significant factors are introduced, which essentially represent Reynolds number, membrane surface area, and accompanying phenomena. This paper explains how these parameters affect the THE performance.

In order to assess the accuracy of the numerical model, a comparison with the experimental data is made. A good conformity between the numerical results and experimental measurements for a designed system is obtained. The originalities of our study are: firstly, the experimental test of incorporated membrane based technology in buildings and its numerical validation under the same experimental conditions, and secondly, the examination of appeared phenomena in Nafion membrane and its impact on both sensible and latent efficiencies.

2. Experimental setup

The experimental setup of the proposed THE is schematically shown in Fig. 1. It consists of three principal components: a hot and humid closed chamber which is modeled as the interior part of the building, a fresh air channel, and a Nafion membrane used to exchange heat and moisture between the two sections. The dimensions of experimental setup, which includes the climate chamber and the fresh air channel, are illustrated in Table 1.

Humid and hot air inside the climate chamber are provided by an electrical stainless steel humidifier to maintain indoor humidity and temperature values of respectively 99.99% and 50 °C. In fact, this work enters in the general framework study dealing with energy recovery from especial building such as Moorish bath where the climate conditions can reach these high values. The humidifier is controlled by an electric heater with an accuracy of 0.1 °C. In the climate chamber, the hot and humid air is initially purged by an external humidifier and then circulated in the whole climate chamber volume using a variable speed fan.

In the current system, the hot and humid air streams periodically adjacent to a Nafion membrane using two ducts inserted in both ends of the climate chamber. On the other hand, heat and

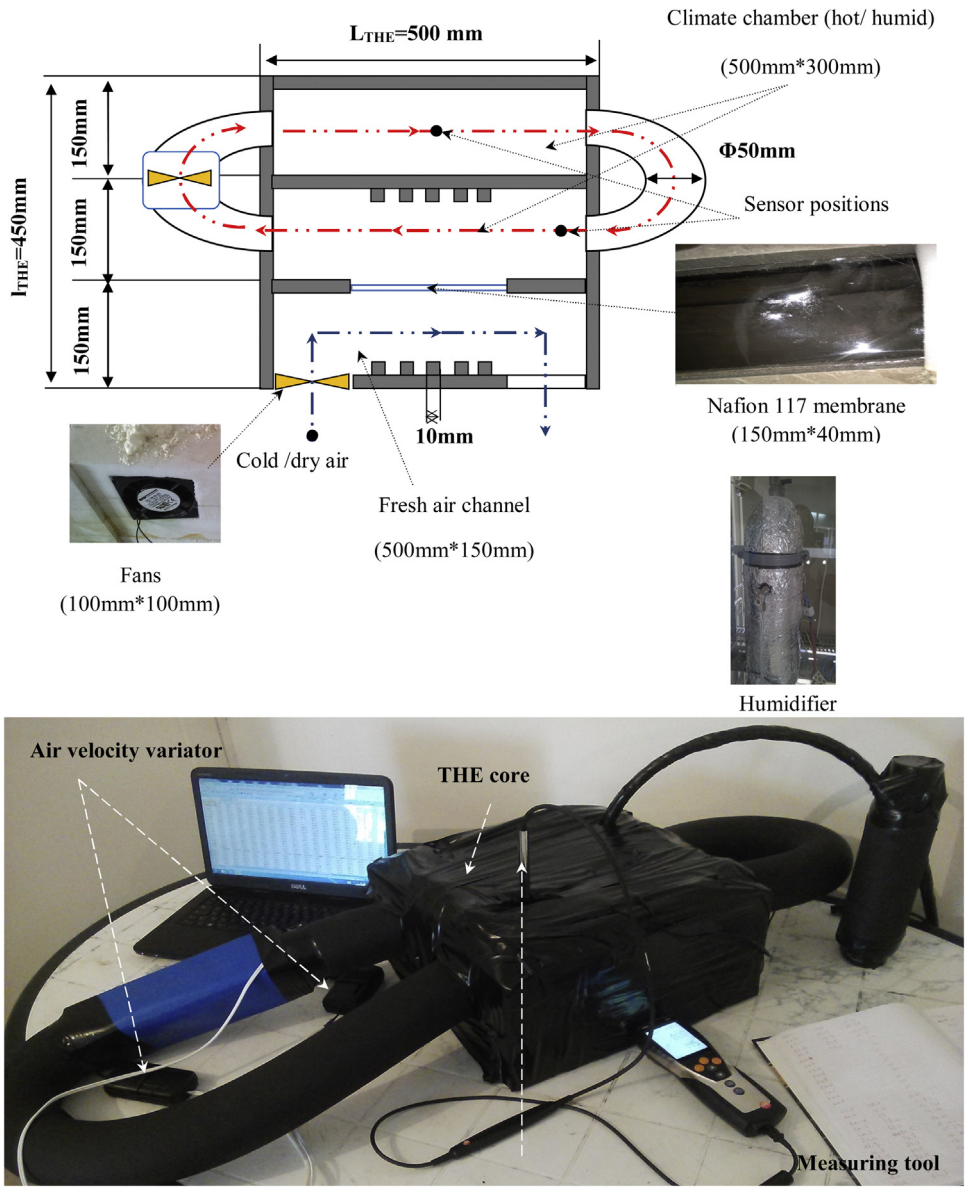

Fig. 1. Schematic description of the experimental setup of the proposed THE.

Table 2
Properties of Nafion 117 membrane.

		Values	Unit
Typical thickness		183	μm
Basis Wight		360	$g\,m^{-2}$
Surface	H_m	$4\ 10^{-2}$	m
S1	L_m	$15\ 10^{-2}$	m
Surface	H_m	$8\ 10^{-2}$	m
S2	L_m	$30\ 10^{-2}$	m

moisture transfer from the inside climate chamber to the external air channel as shown in Fig. 1. This signifies that the combination of an air conditioning system and energy recovery equipment lead to comfortable indoor conditions.

In the base case, Nafion 117 membrane was used to fabricate the proposed system. It has a complex chemical structure formed of a hydrophobic structure and hydrophilic ionic groups in which their properties and dimensions are denoted in Table 2.

The temperature values on the interior chamber are measured by using a type K thin thermocouple with accuracy of 0.1 °C. Humidity ratio in the climate chamber is measured using capacity type humidity transducers with accuracy of 0.1%. The measured values of external and internal air properties are varied during the experimental tests. Furthermore, in order to assess temperature and relative humidity values for each experimental test, measuring control tools have been installed in the internal climate chamber volume as shown in Fig. 1. The dot points represent the sensor positions in the THE system. We have added block obstacles in both ducts in order to improve the heat and mass transfer through the membrane [27].

In order to investigate the effects of exchange surface variation on the THE efficiency, two situations of experiments were carried out. In the first case, the THE efficiency with an active membrane area equal to $6\ 10^{-3}\ m^2$ was studied and corresponding temperature and humidity variation during a time step of 1 min was measured. Accordingly, under the same experimental conditions the analysis was made on the THE using a membrane exchange surface equal to $12\ 10^{-3}\ m^2$. These various membrane dimensions were tested at different internal and external velocities ranging from 0.125 to 0.25 ms^{-1}.

3. Mathematical formulation

The moisture-thermal study in this paper is based on the unsteady two-dimensional model. The following assumptions are made during the modeling of the proposed THE (climate chamber, fresh air channel, and membrane):

- The flows in the whole THE are assumed to be laminar and incompressible.
- The membrane is considered as isotropic and homogeneous porous medium.

A mathematical model involving fluid dynamics and thermodynamic study should consider different operating situations corresponding to the internal and external conditions, which include the fresh air flow in the channel, the hot humid air in the building (climate chamber) and the porous membrane. In this context, mathematical models help to evaluate several mechanisms and operating parameters of THE system.

The transport in the system occurs in the hydrated air channel, the climate chamber, and the membrane. The governing equations for conservation of mass, momentum, energy, and vapor water concentration must be resolved in each region. The dimensionless form in all equations is described by a superscript "*".

The mass conservation equation in 2D is:

$$\frac{\partial u^*}{\partial x^*} + \frac{\partial u^*}{\partial y^*} = 0 \tag{1}$$

Where u*, v* represent the dimensionless velocities.

Conservation of momentum equations can be written as:

$$\frac{\partial u^*}{\partial t^*} + u^*\frac{\partial u^*}{\partial x^*} + v^*\frac{\partial u^*}{\partial y^*} = -\frac{\partial p^*}{\partial x^*} + \frac{1}{\mathrm{Re}}\left[\frac{\partial^2 u^*}{\partial x^{*2}} + \frac{\partial^2 u^*}{\partial y^{*2}}\right] - \varepsilon^2\frac{\nu H}{u_0 K}u^* \tag{2}$$

$$\frac{\partial v^*}{\partial t^*} + u^*\frac{\partial v^*}{\partial x^*} + v^*\frac{\partial v^*}{\partial y^*} = -\frac{\partial p^*}{\partial y^*} + \frac{1}{\mathrm{Re}}\left[\frac{\partial^2 v^*}{\partial x^{*2}} + \frac{\partial^2 v^*}{\partial y^{*2}}\right] - \varepsilon^2\frac{\nu H}{u_0 K}u^* \tag{3}$$

where ε, ν, and u_0 denote respectively the porosity, the kinematic viscosity, and the inlet velocity. *Re*, H, and K are the Reynolds number, height of total heat exchanger, and the membrane permeability, respectively.

In steady state, heat transfer in the THE is modeled by using the energy equation applied to incompressible fluid with constant physical properties (thermal conductivity and diffusivity) and can be written as:

$$\frac{\partial \theta}{\partial t^*} + u^*\frac{\partial \theta}{\partial x^*} + v^*\frac{\partial \theta}{\partial y^*} = \frac{1}{\mathrm{RePr}}\left[\frac{\partial^2 \theta}{\partial x^{*2}} + \frac{\partial^2 \theta}{\partial y^{*2}}\right] \tag{4}$$

Pr represents the Prandtl number.

During moisture transfer process, water vapor molecules are transported through porous membrane by diffusion, caused by water vapor concentration gradient between internal air (inside climate chamber) and fresh air channel [28]. Therefore, the vapor water transport is governed by the following equation:

$$\frac{\partial \xi}{\partial t^*} + u^*\frac{\partial \xi}{\partial x^*} + v^*\frac{\partial \xi}{\partial y^*} = \frac{1}{Sc\mathrm{Re}}\left[\frac{\partial^2 \xi}{\partial x^{*2}} + \frac{\partial^2 \xi}{\partial y^{*2}}\right] \tag{5}$$

Sc represents the Schmidt number for vapor-air mixture. θ and ξ are the dimensionless temperature and humidity ratio, respectively.

The dimensionless temperature and humidity ratio are defined as

$$\theta = \frac{T - T_{fi}}{T_{ei} - T_{fi}} \tag{6}$$

$$\xi = \frac{\omega - \omega_{fi}}{\omega_{ei} - \omega_{fi}} \tag{7}$$

T is the temperature (K) and ω is the humidity ratio ($kg_{vapor}\cdot kg^{-1}{}_{dryair}$). The subscripts "fi" and "ei" refer to inlet fresh air and inlet exhaust air (measured inside the climate chamber), respectively.

The Darcy friction factor and the Reynolds number used to characterize the fluid flow in the duct are given by [2,3],

$$(fRe) = \left(-\frac{D_h\frac{dp}{dx}}{\frac{1}{2}\rho_a u_0^2}\right)\left(\frac{u_0 D_h}{\nu}\right) \tag{8}$$

ρ_a and D_h represent respectively the air density ($kg\,m^{-3}$) and the hydraulic diameter (m).

Due to the small thickness of used membrane (100 μm), some studies have shown that both heat and mass water vapor transfer rates in the x and z directions are considered negligible. Therefore, heat and water vapor transfer equations in the porous membrane can be simplified to one dimensional equation as follow:

$$\frac{\partial^2 \theta_m}{\partial y^{*2}} = 0 \tag{9}$$

$$\frac{\partial^2 \xi_m}{\partial y^{*2}} = 0 \tag{10}$$

3.1. Numerical procedure

Due to the non-linear correlation between the pressure losses and mass transport in the internal climate chamber and gas channel, the magnitude velocity and pressure distributions is calculated using an iterative procedure. A Fortran code is used to solve the coupled governing equations shown in the previous section. The computational domain includes Nafion membrane, external channel and the climate chamber. THE geometrical details and properties are listed in Table 1. Eqs. (1)–(5) are solved numerically by using the volume control method and the Fortran software [29].

The discretized equations, one for each control-volume, are solved by using the successive over relaxation method (SOR) with Chebyshev acceleration. The solution was considered converged when the relative difference between the new and the old values of the considered dependent variables became less than 10^{-6}.

The code includes a subroutine that considers the porous structure effects of the exchanger membrane. The numerical procedure is as follows: (1) boundary conditions, initials conditions and THE parameters in the computational domain are set; (2) the momentum equations are solved without considering pressure effect; (3) Pressure correction is completed in order to consider the mass conservation condition; (4) the transport equations are solved in order to obtain the adequate distribution in all mesh; (5) the calculation procedure is repeated until convergence.

The boundary conditions for the computational domain shown in Fig. 2 are as follows:

Inlet conditions for the fresh air channel:

$$T_{fi} = 25^\circ C;\ \omega_{fi} = 10 g.kg^{-1};\ \theta_{fi} = 0;\ \xi_{fi} = 0$$

Inlet conditions for the climate chamber:

$$T_{ei} = 50^\circ C;\ \omega_{ei} = 20 g.kg^{-1};\ \theta_{ei} = 1;\ \xi_{ei} = 1$$

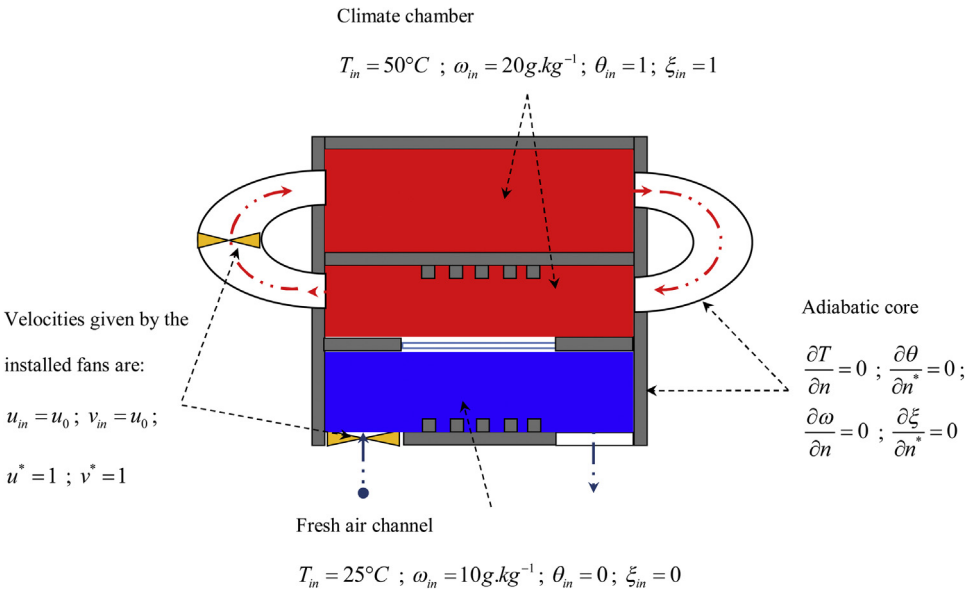

Fig. 2. Schematic description of the boundary conditions in the THE system.

At the THE enclosure:

$$\frac{\partial T}{\partial n} = 0;\ \frac{\partial \theta}{\partial n^*} = 0;\ \frac{\partial \omega}{\partial n} = 0;\ \frac{\partial \xi}{\partial n^*} = 0$$

where n and n* represent respectively the dimension and dimensionless normal vector at boundary.

At the inlet, velocity values are given by the installed fans:

$$u = u_0;\ v = u_0;\ u^* = 1;\ v^* = 1$$

4. Results and discussion

In this section, the test setup is operated under different operating conditions. In order to evaluate their impacts on THE efficiency, the experimental measurements are taken inside the climate chamber for various geometric and operating conditions. In addition, an examination of accompanying phenomena in Nafion membrane is discussed.

4.1. Parameters impacts

4.1.1. Inlet air velocity impact

At the beginning of testing results, the measured air temperature and relative humidity values are: inside climate chamber T_{exp} = 50 °C (323 °K) and RH_{exp} = 99.9% (86 g kg^{-1}); and inlet fresh air channel T_{exp} = 17.2 °C (290.2 °K) and RH_{exp} = 55.4% (7 g kg^{-1}).

Figs. 3 and 4 illustrate the measured temperature and relative humidity values inside the climate chamber for air flow velocities V = 0.125 m s^{-1} and V = 0.25 m s^{-1}.

As can be depicted from Fig. 3, when the air flow velocity increases from V = 0.125 m s^{-1} to V = 0.25 m s^{-1}, the measured air temperature values inside the climate chamber decreases from 19.5 to 17.6 °C. This indicates that the heat transfer rate in the THE enhances under high velocities of circulated air inside climate chamber. Furthermore, we can conclude from Fig. 4 that the relative humidity values inside the climate chamber decreases from 78.3 to 75.2% when the air velocity value increases from V = 0.125 m s^{-1} to V = 0.25 m s^{-1}. It can be explained by the fact that the vapor water is forced to pass through a longer way, air causes remarkable pressure drop and the vapor flows at high velocities, increasing then friction effects which can lead to a better mass transfer. Therefore,

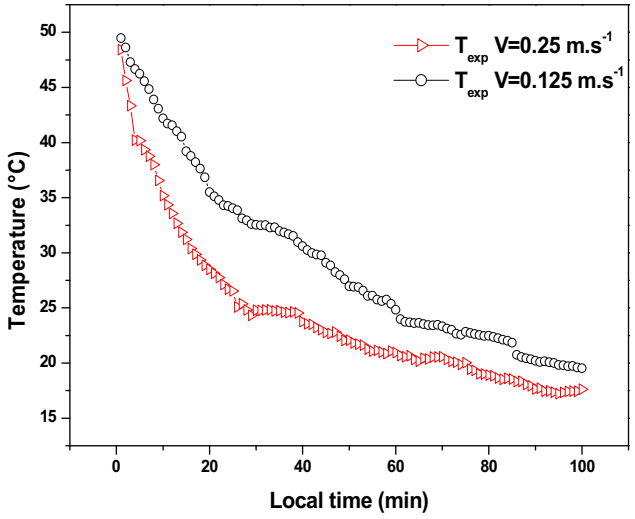

Fig. 3. Measured temperature values inside the climate chamber for air flow velocities V = 0.125 m s^{-1} and V = 0.25 m s^{-1}.

the climate chamber properties depend on climatic and operating conditions such as the external humidity, moisture production, volume flow, and small stationary loss above the climate chamber [21].

For fixed air flow velocity, the relative humidity begins constant, then it decreases and, finally tends to become stable. Fig. 4 shows that the time variation of the relative humidity inside the climate chamber is complicated, because of the appearance of complex physical phenomena such as the activation and clogging of the membrane as discussed in next sections.

4.1.2. Membrane surface impact

The effect of the membrane surface on the THE efficiency was evaluated by considering two dimensions of membrane surface. Figs. 5 and 6 show the tested results of the internal temperature and relative humidity values with two membrane surfaces which are S1 = 6 10^{-3} and S2 = 12 10^{-3} m^2, respectively.

By comparing the test results of membrane surfaces S1 and S2 inside the climate chamber, we can remark that the air temperature

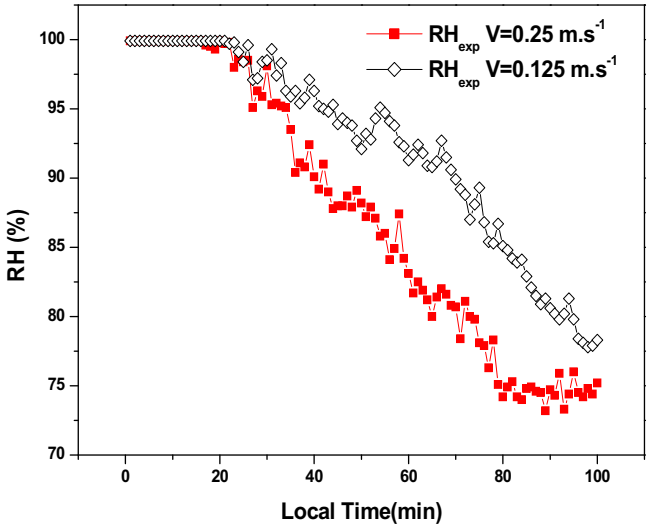

Fig. 4. Measured relative humidity values inside the climate chamber for air flow velocities V = 0.125 m s^{-1} and V = 0.25 m s^{-1}.

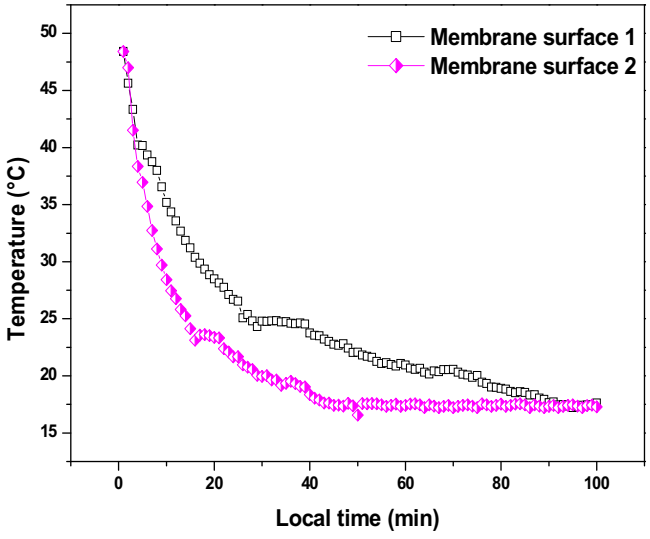

Fig. 5. Measured temperature values inside the climate chamber for membrane surfaces S1 = 6 10^{-3} m^2 and S2 = 12 10^{-3} m^2.

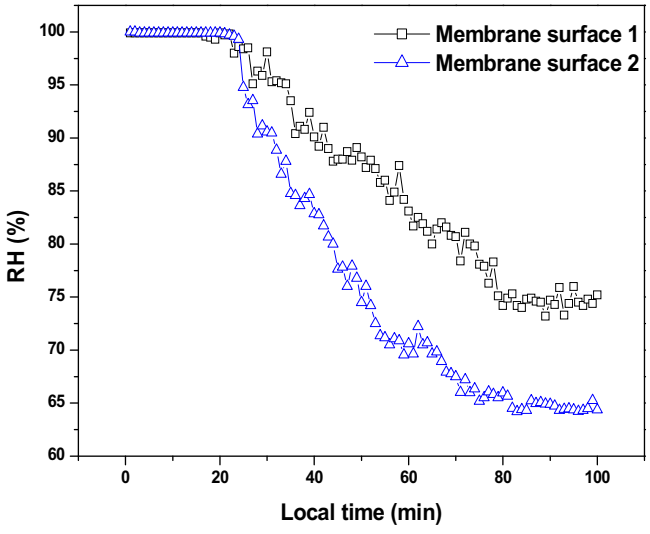

Fig. 6. Measured relative humidity values inside the climate chamber for membrane surfaces S1 = 6 10^{-3} m^2 and S2 = 12 10^{-3} m^2.

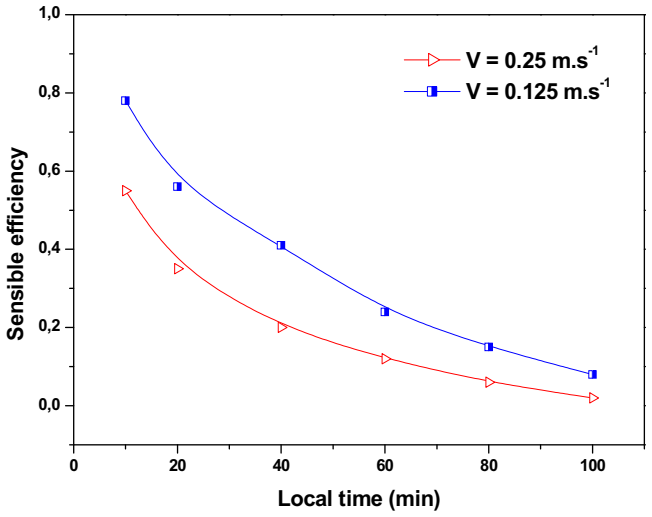

Fig. 7. Calculated sensible efficiency for air flow velocities V = 0.125 m s^{-1} and V = 0.25 m s^{-1}.

and the relative humidity has been improved. Also, the efficiency of THE increases simultaneously with the increase of membrane surface. Furthermore, the time to reach the equilibrium values with membrane surface S2 remains lower than the time with the original membrane surface (S1) at the same air flow rate. It can be seen that the internal relative humidity with membrane surface S2 is reduced by 10% by comparing with the membrane surface S1, as shown in Fig. 6.

The heat and mass transfers are similar for both membrane surfaces S1 and S2. However, the effects on the membrane surface S2 are more significant than the membrane surface S1. The increase of membrane surface leads to a large increase in the surface exchange between the internal and external air streams, causing an increase in the heat and mass transfer rates.

4.1.3. *Performance of total heat exchanger*

In order to evaluate the THE performance, the sensible and latent efficiencies are significant parameters which can be obtained respectively by these expressions:

$$\varepsilon_s = \frac{T - T_{fi}}{T_{ei} - T_{fi}} \quad (11)$$

$$\varepsilon_l = \frac{\omega - \omega_{fi}}{\omega_{ei} - \omega_{fi}} \quad (12)$$

where T_{ei} and ω_{ei} represent the measured temperature and humidity ratio values inside the climate chamber at the beginning (t = 0 min) and are equals to T_{ei} = 50 °C and ω_{ei} = 86 g kg^{-1} (99.9%), respectively. In addition, T_{fi} and ω_{fi} are the measured fresh air temperature and humidity ratio values at the inlet (t = 0 min) which are equal to 17.2 °C and 7 g kg^{-1} (55.4%), respectively. T and ω represent the measured temperature and humidity ratio values inside the climate chamber at different time of experimentation.

As the Reynolds number increases, the pressure difference between internal and external buildings (climate chamber) increases, leading to a larger driving force for air through the porous membrane surface. Fig. 7 shows the effect of the inlet air velocity on the sensible efficiency of THE. It is observed that the calculated sensible efficiency decreases progressively with elapsed time and also it is a decreasing function of inlet air velocity. The decrease of sensible efficiency is usually caused by the decrease of the heat transfer rate in THE system.

Fig. 8 shows the calculated latent efficiency of THE for different air flow velocities. As can be seen, by varying the air velocity

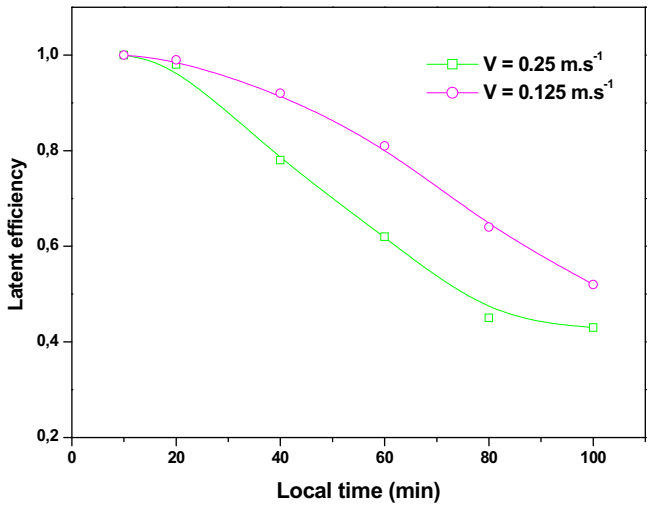

Fig. 8. Calculated latent efficiency for air flow velocities V = 0.125 m s^{-1} and V = 0.25 m s^{-1}.

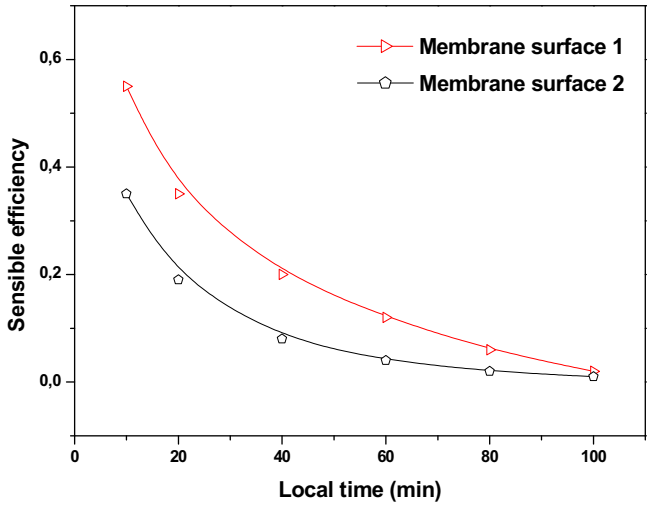

Fig. 9. Calculated sensible efficiency for membrane surfaces S1 = 6 10^{-3} m^2 and S2 = 12 10^{-3} m^2.

from 0.125 m s^{-1} to 0.25 m s^{-1}, the figure shows a slight decrease in latent efficiency of 15% at test time t = 40 min, and 20% at test time t = 80 min, respectively.

The appearance of the constant phase at the beginning of latent efficiency can be explained by the fact that the porous membrane under the test conditions is momentary in the activation time. Then, the latent efficiency is gradually decreased with decrease of moisture transport rate between the internal air (inside climate chamber) and fresh air streams. This decrease of latent efficiency is due to the progressively reduction of the mass transfer rate which is controlled at last by the obstruction phenomenon, known as membrane clogging.

Furthermore, in order to appreciate the THE efficiency under various membrane surface, Figs. 9 and 10 are plotted. As depicted from Fig. 9, at test time t = 20 min, the sensible efficiency decreases by 15%, however it reduces only by 8% at test time t = 60 min. On the other hand, the latent efficiency decreases from 0.78 to 0.62 at test time t = 40 min, however at test time t = 80 min it decreases from 0.45 to 0.23 as shown in Fig. 10. By increasing the surface of porous membrane, both sensible and latent efficiencies decrease gradually with the test time. This signifies that heat and mass transfer through tested Nafion membrane are affected by other parameters [1].

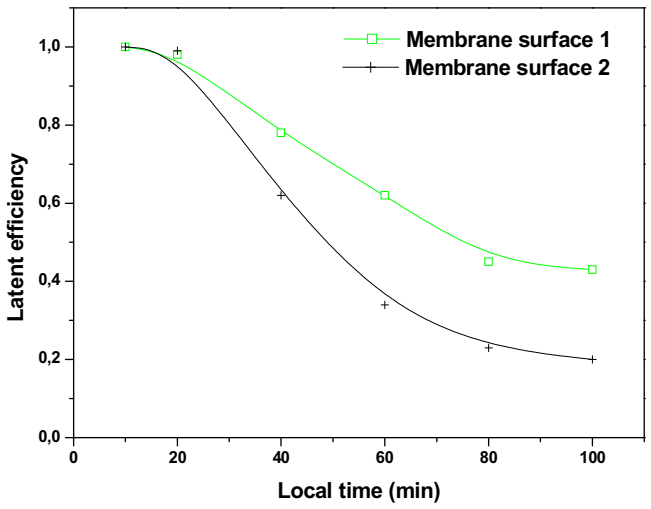

Fig. 10. Calculated latent efficiency for membrane surfaces S1 = 6 10^{-3} m^2 and S2 = 12 10^{-3} m^2.

4.2. Membrane phenomena

4.2.1. Membrane activation

The Nafion membrane is composed of hydrophobic backbone and hydrophilic ionic groups which can be the main source of appearance of this physical phenomenon. Chemically, their ionic groups trap the first vapor water molecules to dissociate responsible protons of ionic membrane conductivity. In order to explain the effects of geometric and operating parameters on the porous membrane property as well as the observable phenomena in the test results, an activation time is discussed. The activation time represents the moment at which the moisture transfer starts and progresses through the porous membrane.

We can conclude from Fig. 11a and Fig. 11b that the porous membrane takes several minutes for moisture transport to reach unsteady state for various geometric and operating parameters. By increasing the membrane surface, the activation time of porous membrane increases from 20 to 24 min. This signifies that the small surface of membrane takes lower time to enable water vapor to cross. On the other hand, the steady response of the relative humidity inside climate chamber (activation time) decreases from 21 to 17 min when the air flow velocity varies from = 0.125 m s^{-1} to V = 0.25 m s^{-1}. Therefore, the increase of air flow velocity makes the moisture transfer more rapid through the porous Nafion membrane as shown in Fig. 11b.

After activation time, the moisture is gradually rejected out. At the end, the relative humidity returns to another steady period which is explained by the complex phenomenon, known as membrane clogging [30].

4.2.2. Membrane clogging

The membrane clogging is due to the particles accumulation in the membrane surface which reduces its permeability. This accumulation is constituted of particles, colloids and bacteria. Clogging of membrane is a complex phenomenon and it greatly depends on the membrane characteristics such as porosity, thickness and permeability. Hermia [31] proposed a model based on four ideal mechanisms to describe the membrane clogging. These mechanisms are:

- Cake layer formation in which the particles collect along the membrane surface and then constitute an additional surface.
- Imposed pore sealing in which only few particles at the membrane surface contribute to the blocking of pores.

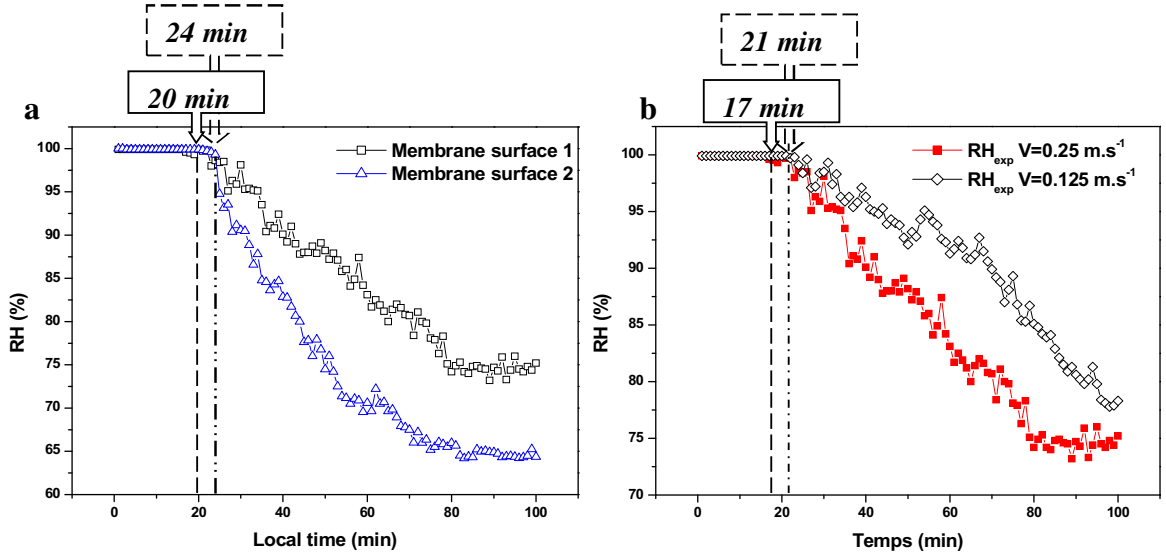

Fig. 11. Measured activation time of Nafion membrane for: a. Membrane surfaces S1 = 6 10^{-3} m^2 and S2 = 12 10^{-3} m^2, and b. Air flow velocities V = 0.125 m s^{-1} and V = 0.25 m s^{-1}.

- Pore restriction in which the small particles are deposited within the pores and reduce their effective diameter.
- Pore sealing in which all the particles at the membrane surface contribute to complete clogging.

The clogging time represents the moment at which the clogging phenomenon starts in progress. Fig. 12a shows the clogging time of the Nafion membrane measured at the experimental test for air velocity ranging from V = 0.125 m s^{-1} to V = 0.25 m s^{-1}. We remark that the clogging time decreases from 95 to 80 min when Reynolds number varies from 31 to 62. Therefore, as the air velocity increases, the clogging time declines. An increase of inlet air velocity means that there is vapor water through the porous membrane which leads to a large membrane obstruction and THE efficiency decreases.

Fig. 12b illustrates the clogging time under various membrane surfaces. The analysis is carried out by varying the surface of membrane in THE but keeping the other operating variables constant. As shown, the measured clogging time increases with increasing membrane surface due to higher pores number in the Nafion membrane [28,30]. We can remark that the increase of membrane surface leads to delay the starting of clogging phenomenon.

To achieve high performance, the amount of water content in the climate chamber should be in a suitable range to allow the delay of the clogging phenomenon and to enhance the transportation of water vapor.

5. Numerical validation

In order to examine the numerical model of THE, a comparison with our experimental data is established. This comparison carried out under inlet operating conditions: inside climate chamber T_{exp} = 50 °C (323 K) and RH_{exp} = 99.9% (86 g kg^{-1}); and fresh air channel T_{exp} = 17.2 °C (290.2 °K) and RH_{exp} = 55.4% (7 g kg^{-1}).

The key elements in the THE modeling are the transport phenomena through porous membrane, the climate chamber and fresh air channel properties.

Figs. 13 and 14 show the comparison between numerical results and experimental data of the climate chamber. As can be seen in Fig. 13, the numerical relative humidity of the air in the climate chamber decreases linearly from 99.99 to 75% for air velocity value V = 0.25 m s^{-1}. However, three regions are observed in the measured relative humidity profile which begins by a constant region (membrane activation) then reduces gradually to finish with another constant region due to the effect of membrane clogging.

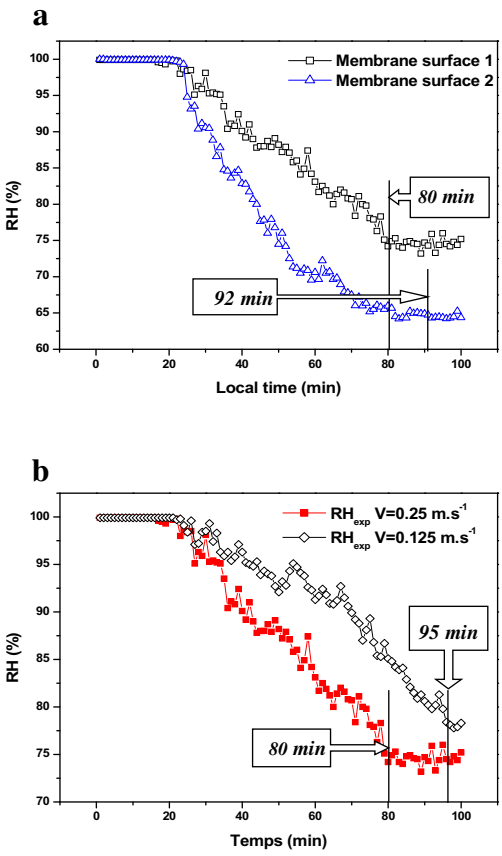

Fig. 12. Measured clogging time of Nafion membrane for: a. Membrane surfaces S1 = 6 10^{-3} m^2 and S2 = 12 10^{-3} m^2, and b. Air flow velocities V = 0.125 m s^{-1} and V = 0.25 m s^{-1}.

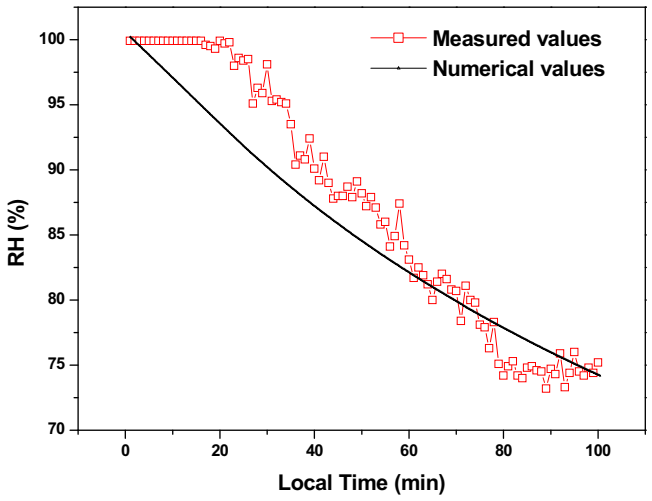

Fig. 13. Comparison between measured and numerical relative humidity values inside the prototype building.

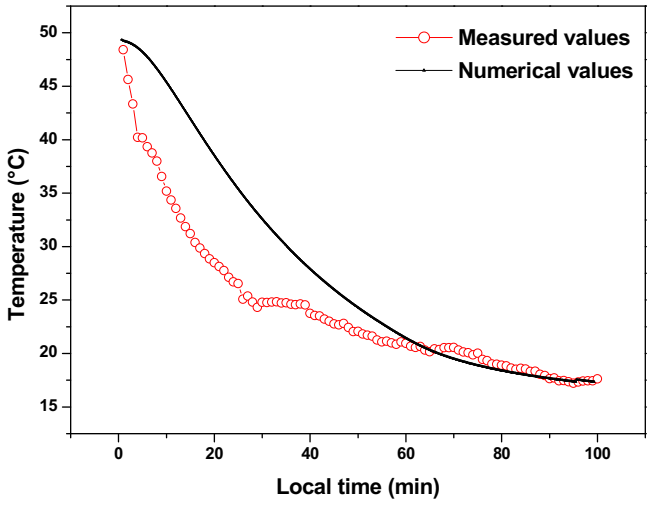

Fig. 14. Comparison between measured and numerical temperature values inside the climate chamber.

Fig. 14 shows a comparison between temperature results obtained from both numerical model and experimental work. We can remark that the air temperature reduces steadily to reach the same outside fresh air temperature value. The experimental temperature profile is similar to the mean temperature predicted by numerical model which decreases slowly to reach the final experimental value (17 °C).

In the validation part, the results can be discussed into two distinguished points:

- Generally, these previous results show that the experimental and numerical profiles have the same trends and then the accuracy is acceptable.
- Discrepancies between the experimentation and calculation results are essentially due to the presence of physics phenomena (activation and clogging) and the effects of water condensation.

The numerical model is generally in agreement with the experimental data. This global accord allows us to investigate the general aspects of parameters effects on the THE efficiency. However, the numerical model must take account the appearance of membrane phenomena such as activation and clogging of Nafion membrane. This indicates that the appeared phenomena should be investigated in particular studies. A research project, in progress, carries to study the appeared phenomena in porous membrane in order to examine and to validate these previous results under diverse conditions as well as to approve the consistency of the developed numerical model (Fig. 14).

6. Conclusion

The total heat exchanger is experimentally investigated. Tests are done using Nafion membrane. The measurements inside a climate chamber are evaluated for various test conditions. The impacts of air flow velocity and membrane surface effects on the heat and mass transfer rates are experimentally investigated. Experimental phenomena such as activation and clogging of membrane are evaluated. The momentum, energy and mass transport equations are developed to describe the flow, heat and mass transfer in the considered THE. A numerical validation is established by a comparison between our numerical and experimental results. Therefore, the following results have been established:

- An increase in air flow velocity enhances heat and mass transfer between the fresh air channel and the inside climate chamber as well as the sensible and latent efficiencies.
- The surface of membrane has a great impact on the temperature and humidity profiles inside the climate chamber when it is sufficiently large. Therefore, a high membrane surface leads to large sensible and latent efficiencies.
- The variation of membrane surface and/or flow velocity has an important impact on the activation and clogging times of Nafion membrane.

The activation and clogging of membrane are complex phenomena which must particularly be studied by specific numerical model with surface characterization which is our research project in progress.

References

[1] A. Mardiana-Idayu, S.B. Riffat, An experimental study on the performance of enthalpy recovery system for building applications, Energy Build. 43 (2011) 2533–2538.
[2] M. Nasif, R. AL-Waked, G. Morrison, M. Behnia, Membrane heat exchanger in HVAC energy recovery systems, systems energy analysis, Energy Build. 42 (2010) 1833–1840.
[3] R. Al-Waked, M.S. Nasif, G. Morrison, M. Behnia, CFD simulation of air to air enthalpy heat exchanger, Energy Convers. Manage. 74 (2013) 377–385.
[4] X.R. Zhang, L.Z. Zhang, H.M. Liu, L.X. Pei, One-step fabrication and analysis of an asymmetric cellulose acetate membrane for heat and moisture recovery, J. Membr. Sci. 366 (2011) 158–165.
[5] M. Gandiglio, A. Lanzini, M. Santarelli, P. Leone, Design and optimization of a proton exchange membrane fuel cell CHP system for residential use, Energy Build. 69 (2014) 381–393.
[6] D.T. Bui, A. Nida, K.C. Ng, K.J. Chua, Water vapor permeation and dehumidification performance of poly(vinyl alcohol)/lithium chloride composite membranes, J. Membr. Sci. 498 (2016) 254–262.
[7] P. Liu, M.R. Nasr, G. Ge, M.J. Alonso, H.M. Mathisen, F. Fathieh, C. Simonson, A theoretical model to predict frosting limits in cross-flow air-to-air flat plate heat/energy exchangers, Energy Build. 110 (2016) 404–414.
[8] J. Min, J. Duan, Membrane-type total heat exchanger performance with heat and moisture transferring in different directions across membranes, Appl. Therm. Eng. 91 (2015) 1040–1047.
[9] Q. Zhong, L. Yang, Y. Tao, C. Luo, Z. Xu, T. Xi, An optimized cross flow plate-fin membrane-based total heat exchanger, Energy Build. 86 (2015) 550–556.
[10] X.H. Ye, M.D. Levan, Water transport properties of nafion membranes. Part I. Single-tube membrane module for air drying, J. Membr. Sci. 221 (2003) 147–161.
[11] A.A. Al-Farayedhi, P. Gandhidasan, S.Y. Ahmed, Regeneration of liquid desiccants using membrane technology, Energy Convers. Manage. 40 (1999) 1405–1411.
[12] L. Dilandro, M. Pegoraro, L. Bordogna, Interaction of polyether-polyurethane with water vapor and water-methane separation selectivity, J. Membr. Sci. 64 (1991) 229–236.

[13] P. Scovazzo, A. Hoehn, P. Todd, Membrane porosity and hydrophilic membrane based dehumidification performance, J. Membr. Sci. 167 (2000) 217–225.
[14] P. Aranda, W.J. Chen, C.R. Martin, Water transport across polystyrenesulfonate/alumina composite membranes, J. Membr. Sci. 99 (1995) 185–195.
[15] X.R. Zhang, L.Z. Zhang, H.M. Liu, L.X. Pei, One-step fabrication and analysis of an asymmetric cellulose acetate membrane for heat and moisture recovery, J. Membr. Sci. 366 (2011) 158–165.
[16] L.Z. Zhang, Y.Y. Wang, C.L. Wang, H. Xiang, Synthesis and characterization of a PVA/LiCl blend membrane for air dehumidification, J. Membr. Sci. 308 (2008) 198–206.
[17] X. Ye, M.D. LeVan, Water transport properties of nafion membranes: part I. Single-tube membrane module for air drying, J. Membr. Sci. 221 (2003) 147–161.
[18] M. Yang, S.M. Huang, X. Yang, Experimental investigations of a quasi-counter flow parallel-plate membrane contactor used for air humidification, Energy Build. 80 (2014) 640–644.
[19] P. Buzatu, T. Zsirai, P. Aerts, S.J. Judd, Permeability and clogging in immersed hollow fibre membrane bioreactor, J. Membr. Sci. 421–422 (2012) 342–348.
[20] H.S. Kandra, D. Mac Carthy, T.D. Fletcher, A. Deletic, Assessment of clogging phenomena in granular filter media used for stormwater treatment, J. Hydrol. 512 (2014) 518–527.
[21] A. Korjenic, T. Bednar, An analytical solution of a moisture transfer problem for coupled room and building component, Energy Build. 47 (2012) 254–259.
[22] A. Vali, G. Ge, R.W. Besant, C.J. Simonson, Numerical modeling of fluid flow and coupled heat and mass transfer in a counter-cross-flow parallel-plate liquid-to-air membrane energy exchanger, Int. J. Heat Mass Transfer 89 (2015) 1258–1276.
[23] M.I. Nizovtsev, V.Y. Borodulin, V.N. Letushko, A.A. Zakharov, Analysis of the efficiency of air-to-air heat exchanger with a periodic change in the flow direction, Appl. Therm. Eng. 93 (2016) 113–121.
[24] J. Min, L. Wang, Coupled heat and mass transfer during moisture exchange across a membrane, J. Membr. Sci. 430 (2013) 150–157.
[25] J. Min, T. Hu, Y. Song, Experimental and numerical investigations of moisture permeation through membranes, J. Membr. Sci. 367 (2011) 174–181.
[26] M. Rasouli, S. Akbari, C.J. Simonson, R.W. Besant, Energetic, economic and environmental analysis of a health-care facility HVAC system equipped with a run-around membrane energy exchanger, Energy Build. 69 (2014) 112–121.
[27] S. Sabek, F. Tiss, R. Chouikh, A. Guizani, Numerical investigation of membrane based heat exchanger with partially blocked channels, Appl. Therm. Eng. 104 (2016) 203–211.
[28] P.W. Majsztrik, M.B. Satterfield, A.B. Bocarsly, J.B. Benziger, Water sorption, desorption and transport in nafion membranes, J. Membr. Sci. 301 (2007) 93–106.
[29] T. Faysal, R. Chouikh, A. Guizani, A numerical investigation of reactant transport in a PEM fuel cell with partially blocked gas channels, Energy Convers. Manage. 80 (2014) 32–38.
[30] M. Moaddeb, W.J. Koros, Occlusion of pores of polymeric membranes with colloidal silica, J. Membr. Sci. 136 (1997) 273–277.
[31] J. Hermia, Constant pressure blocking filtration laws—application to power law non Newtonian fluids, Trans. Inst. Chem. Eng. 60 (3) (1982) 183–187.